Adsorption and Coupling of 4-aminophenol on Pt(111) surfaces

G. Otero-Irurueta[1,2], **J. I. Martínez**[1], **R.A. Bueno**[1], **F. J. Palomares**[1], **H. J. Salavagione**[3], **M. K. Singh**[2], **J. Méndez**[1], **G. J. Ellis**[3], **M. F. López**[1], and **J. A. Martín-Gago**[1,*]

[1]ESISNA Group, Dept. Surfaces, Coatings and Molecular Astrophysics, Institute of Material Science of Madrid (ICMM-CSIC), Sor Juana Inés de la Cruz 3, 28049 Madrid, Spain

[2]Center for Mechanical Technology and Automation (TEMA), Department of Mechanical Engineering, University of Aveiro, 3810-193 Aveiro, Portugal

[3]Polymer Physics Group, Dept. Polymer Physics, Elastomers and Energy Applications, Institute of Polymer Science and Technology (ICTP-CSIC), Juan de la Cierva 3, 28006 Madrid, Spain

Abstract

We have deposited 4-aminophenol on Pt(111) surfaces in ultra-high vacuum and studied the strength of its adsorption through a combination of STM, LEED, XPS and *ab initio* calculations. Although an ordered (2 3×2 3)R30° phase appears, we have observed that molecule-substrate interaction dominates the adsorption geometry and properties of the system. At RT the high catalytic activity of Pt induces aminophenol to lose the H atom from the hydroxyl group, and a proportion of the molecules lose the complete hydroxyl group. After annealing above 420K, all deposited aminophenol molecules have lost the OH moiety and some hydrogen atoms from the amino groups. At this temperature, short single-molecule oligomer chains can be observed. These chains are the product of a new reaction that proceeds via the coupling of radical species that is favoured by surface diffusion.

Keywords

aminophenol; oligomer; STM; DFT; Pt(111); on-surface synthesis

1 Introduction

On-surface synthesis is growing to become one of the most promising strategies for producing new macromolecules or 2D extended nanostructures [1]. In recent years, different well-known chemical reactions have been tested on metallic surfaces [2–6] with the aim of: i) obtaining a deep insight into the chemical pathways that reactants follow, and ii) obtaining new molecular species with targeted functionalities [3]. Among others, covalent coupling between reactants has become especially interesting because of the high level of thermal and chemical stability of the target nanostructures [4–13]. The on-surface synthesis process starts with the adsorption on the substrate of the molecular precursor or building block. The interaction of these with the surface is a key point to understand the nature of the final

reaction products [3]. During recent years different metal-catalysed chemical coupling reactions have been deeply studied by the group of Lambert [14–17]. They succeeded in forming new C–C bonds in a Sonogashira-type coupling leading to the formation of new aromatic species on very different surfaces. Particularly, they described new surface-induced enantioselective catalytic routes that could have a key impact both in the research laboratory and in the production of chemicals and pharmaceuticals [14–15]. Here we focus on the formation of short oligomeric chains through coupling of radicalized amino groups.

Aminophenol is both a simple and interesting molecule. It consists of a single aromatic ring with two different functional groups (-NH$_2$ and –OH) and can exist in three isomeric forms, with the amine group in positions *ortho-* (*2-*), *meta-* (*3-*) and *para-* (*4-*) with respect to the OH group on the aromatic ring. These functional groups provide ideal sites for the formation of larger nanostructures by means of different assembly mechanisms, ranging from simple intermolecular interactions to the formation of covalent linkages. The type and extent of molecular assembly critically depends on the isomer configuration, and to date covalent molecular systems from aminophenol building blocks have mainly been achieved using electrochemical tools on Pt electrodes. [18,19]

In the present work, with the help of a synergistic combination of STM, LEED and XPS techniques with *ab-initio* calculations, we report on the formation of extended single-molecule structures on a Pt(111) surface built from para-aminophenol (4AP) building-blocks under ultra-high vacuum (UHV) conditions. Platinum was preferentially chosen as the metal substrate due to its well-known catalytic properties, in particular the promotion of successive on-surface chemical reactions [20] and since it has also been previously used as a working electrode for electrochemical polymerization [18]. In the first instance we focus on the adsorption of 4AP on Pt(111), where we show that the molecular surface interaction dominates over the molecule-molecule interaction. Then we describe the thermal coupling of 4AP building-blocks, where we demonstrate that the 4AP molecules react together on the Pt(111) surface, and present a conceptual model to explain the nature of the processes involved.

2   Methods

2.1   Experimental Section

The experiments were undertaken in two UHV systems, the first equipped with room temperature (*RT*) STM and LEED, while the second was used for XPS characterization.

The Pt(111) substrate was cleaned by repeated cycles of argon sputtering (10 min) and annealed at 1200 K in an oxygen atmosphere (10 min, P=5×10^{-8} mbar). After three cycles under these conditions several extra cycles without oxygen were performed in order to completely remove any remaining contaminants from the Pt surface. The surface cleanliness was then verified using STM and LEED.

4-aminophenol (4AP) (Sigma-Aldrich, powder, 99%, CAS No. 123-30-8) was introduced into a quartz container located in a pre-chamber with an independent pumping system and a base pressure of 1×10^{-9} mbar, degassed for several hours at 320 K and sublimated at 350 K.

A heater surrounded the molecular container, and a thermocouple were directly fixed to the external wall of the container in order to guarantee the reproducibility of the sublimation conditions. For the molecular deposition on the platinum surface the valve separating the pre-chamber from the main system was completely opened.

After molecular deposition the surface was characterized by LEED and *RT*-STM in the same system used for growing the molecular layer. After sample transfer under UHV conditions to the second main chamber, XPS measurements were undertaken. Omicron RT-STM with WSxM electronic and software was used for data acquisition and analysis [21].

XPS was used to characterize the composition and chemical evolution of the sample *in-situ* through consecutive annealing steps. XPS spectra were acquired in an UHV chamber with a base pressure of 10^{-9} mbar equipped with a hemispherical electron energy analyzer (SPECS Phoibos 150 spectrometer) and a delay-line detector in the nine-segment mode, using a monochromatic AlKα (1486.74 eV) X-ray source. Spectra were recorded at normal emission take-off angle, using an energy step of 0.1 eV and a pass-energy of 20 eV, which provide an overall instrumental peak broadening of 0.5 eV.

2.2 Theoretical Section

2.2.1 Computational details—For the *ab initio* atomistic and molecular dynamics simulations of the different proposed models analyzed in this study, Density Functional Theory (DFT) was used effectively combining the localized-basis set and plane-wave schemes as implemented in the FIREBALL [22] and QUANTUM ESPRESSO [23] simulation packages, respectively, accounting for a perturbative van der Waals (vdW) correction to validate the reliability of the different adsorbed molecules and adlayer configurations. To this purpose an empirical efficient vdW R^{-6} correction was used to add dispersive forces to conventional density functions (DFT+D) [24,25]. The exchange-correlation (XC) effects have been accounted for by using the local density PW91 parametrization [26], and norm-conserving scalar-relativistic pseudo-potentials [27] have been considered to model the ion-electron interaction.

For the localized-basis set code FIREBALL, a sp^{3}d^{5}d^{*5} basis set of single and double numerical atomic orbitals was employed for Pt, a double numerical sp^{3}s*p^{*3} basis set for H and O, and optimal polarized sp^{3}d^5 basis sets for C and N. For the plane-wave code QUANTUM ESPRESSO, a plane-wave basis set with a kinetic energy cutoff of 500 eV was used. In all the calculations the Brillouin zone (BZ) was sampled by means of optimal Monkhorst-Pack grids [28], guaranteeing full convergence in energy and electronic density. The atomic relaxations were carried out with a conjugate gradient minimization scheme, until the maximum force on any atom was below 0.01 eV Å^{-1}. The Fermi level was smeared using the Methfessel-Paxton approach [29] with a Gaussian width of 0.01 eV, and all energies were extrapolated to T = 0 K. All these parameters yield energies with an accuracy of E $\approx \pm$ 0.01 eV (converged to a precision better than 10^{-6} eV).

2.2.2 Theoretical STM-imaging—In our STM approach, tunneling currents for the STM images have been calculated using a Keldysh–Green function formalism, together with the first-principles tight-binding Hamiltonian obtained from the local-orbital DFT-

FIREBALL method (as explained in detail elsewhere [22,30,31]). In order to obtain accurate STM images and tunneling currents, to be compared with our experimental UHV-STM images, we used an efficient STM theoretical simulation technique that includes, by construction, a detailed description of the electronic properties of both the tip and the sample. With this technique the system is divided into "sample" and "tip", where the samples correspond to the different proposed interfacial models. In these calculations to simulate the scanning we have assumed a tungsten (W) tip configuration formed by 5 protruding atoms (one at the apex) attached to an extended W(100)-crystal. The overlapping Hamiltonian is obtained by using a dimer approximation: a dimer formed by one W atom (corresponding to the tip) and another (H, C, N, O and Pt coming from the sample) is calculated for different atom–atom distances and for all the non-zero interactions, using the Keldish-Green formalism to propagate the tunnel current between both subsystems [22,30,31]. All the theoretical STM images have been obtained at constant-current scanning conditions, moving the W-tip perpendicularly to the sample in each scanning stage to search a pre-selected fix value of the tunnel current in order to mimic experimental procedure.

2.2.3   Models—To construct the system geometries used in the calculations we have considered: *i*) a slab of four physical Pt(111) layers with a minimum distance of ~ 25 Å of vacuum between neighbouring cells along the axis perpendicular to the surface; as well as *ii*) full periodic boundary conditions representing infinite Pt(111) surfaces. Each substrate metal layer contained 16 and 12 Pt atoms for the dilute (4×4) and the close-packed (2 3×2 3)R30° configurations, respectively, with unit cells of size (11.3×11.3) Å^2 and (9.7×9.7) Å^2 each containing one 4AP molecule. Only the two bottom Pt(111) physical layers were fixed, and two additional Pt(111) layers were accounted for in the calculations of the energetics, electronic structure, and theoretical STM-imaging. The Brillouin zone (BZ) was sampled by means of [4×4×1] and [6×6×1] Monkhorst-Pack grids for the dilute (4×4) and the close-packed (2 3×2 3)R30° configurations, respectively, guaranteeing full convergence in energy and electronic density.

3   Results and Discussion

4AP molecules were initially deposited on the Pt(111) surface at 300K (RT) up to saturation coverage, and Figure 1 shows STM images subsequently acquired. At this temperature individual molecules can be clearly distinguished appearing scattered over the surface and producing a homogenous layer. The molecules appear in the STM images as elongated features that exhibit a long and a short axis with lengths of (8.5±0.5) Å and (5.5±0.5) Å, respectively. At low-coverage the molecules appear randomly distributed on the flat Pt(111) terraces, but as the coverage is increased the STM images show small regions where the molecules form ordered domains (see central part of Figure 1c,). A detailed inspection of LEED patterns at different electron energies (Figure 1b), shows the emergence of a faint (2 3×2 3)R30° pattern, indicating that the structural periodicity includes some disarray .Typically, the observed islands are formed with no more than 30 molecules, as is the case shown in the central part of Figure 1. It is important to remark that increasing the molecular dose by a factor of ten produced no increase in the coverage of the sample at this temperature, and thus Figure 1 corresponds to saturation coverage.

By considering the long axis of the molecules (Figure 1d, solid red lines superimposed on the molecules) we can establish their on-surface orientation with respect to the main crystallographic directions of the Pt(111) substrate (defined by LEED). Interestingly, a close inspection of the high-resolution STM images reveals that the molecules are not randomly oriented, but they all appear to be aligned with their long axis at an angle of 30° with respect to the main crystallographic directions of the Pt(111) surface (see inset at the bottom of figure 1d).

Importantly, the STM images in Figure 1 allow us to distinguish two different morphologies with regard to the internal structure of 4AP molecules on Pt(111) (see top-left insets in panels c and d). Some molecules exhibit a "one-blob" internal structure (top-left inset in Figure 1c), whilst others show a "two-blob" structure, one of the blobs being slightly larger than the other (top-left inset Figure 1d). We notice that albeit this variability the STM images do not visibly depend on the bias voltage (from -2000 mV to +2000 mV), but the shape and height of the main bodies are very similar for both types of molecule. Thus, an average apparent height of (0.9 ± 0.1) Å can be statistically derived. This value is compatible with the central aromatic ring in a parallel geometry to the surface, in agreement with other reported examples of related molecules like phenol, aniline or tetra-amino benzene on metallic surfaces [32–36]. Moreover, large polycyclic aromatic hydrocarbons (PAHs), mainly formed by benzene like rings have an apparent height of less than 2 Å in a planar configuration parallel to the surface [3,37]. At a first glance, the difference detected in the internal structure of the molecules could be ascribed to two different adsorption configurations on the Pt surface (a structural effect) and / or to a reorganization of the electronic structure due to a chemical change in the molecule.

XPS experiments provide important evidence for chemical changes that occur in the molecules allowing a clearer understanding of the STM images. Figure 2 shows that at RT, the O 1s spectra can be fitted by a single component centered at a binding energy (BE) of (531.0 ± 0.1) eV. This suggests that all oxygen atoms are equivalent. Ihm *et al.* reported a BE of 532.2 eV for a related molecule, phenol, on the same substrate at low temperature. Moreover, the same authors indicated that the first typical reaction that takes place in similar molecules on metals upon heating is the cleavage of the O-H bond [38]. Importantly, that reaction is thermally activated at around 180 K, a lower temperature than our working conditions (RT). Thus, by considering all this information we can ascribe the peak detected at 531 eV in our experiments with a –C=O chemical environment [39,40]. Consequently, XPS indicates that upon adsorption of the molecules on the Pt(111) surface at RT, the H atoms are lost from the hydroxyl groups. The N 1s spectra obtained by XPS at RT can be fitted by a single component centered at a BE of (399.6 ± 0.1) eV (lower spectra of Figure 2b). Recently, a BE of 399.9 eV was reported for the N 1s component of the amino groups of tetra-amino benzene molecules on Cu(111) [36] and a BE of 399.8 eV was reported for amine groups of *p*-phenylenediamine on Ag(111). [41] Thus, in our case we ascribe the observed peak to the amino group of 4AP molecules on the Pt(111) surface.

In order to shed some light on the structure and interaction of the 4AP molecules deposited on Pt(111), as well as to elucidate the origin of the two different molecule types observed in the STM images at RT, we have undertaken a battery of DFT+D calculations. Initially,

according to the XPS and STM evidences, we have considered the isolated molecule after the hydroxyl groups have lost the hydrogen atoms, and arranged the 4AP molecules on the surface with molecular axis directions forming an angle of 30° with respect to the main Pt(111) crystallographic directions, employing a unit cell sufficiently large (4×4) to ensure that a molecule does not "see" the neighbouring one.

Three non-equivalent starting configurations were fully relaxed: that with the central aromatic ring of the AP molecule lying i) on-top, ii) on a surface Pt-Pt bridge, and iii) on a surface hollow site. The result of the calculations reveals that the 4AP molecules (with no hydrogen atom in the hydroxyl group) are most stable when adopting the second configuration, at the bridge adsorption site, and are found to be lying flat on the surface at a perpendicular distance of around 2.07 Å between the lowest C atoms and the Pt substrate (see left-top panel of Fig. 3). From the theoretical optimization, the long axis remains parallel to a direction forming a 30° angle with the main crystallographic directions of Pt(111), without any azimuthal reorientation after the process. The adsorption energy for this configuration can be estimated as -1.78 eV per molecule (the negative value for the adsorption energy, by construction, means that the adsorption is favorable and stable). DFT +D calculations show that the origin of this interaction is quite chemical, and covalent bonds arise between C and N atoms of the 4AP molecules and the Pt atoms of the substrate. Nevertheless, the intrinsic nature of this interaction does not modify substantially the structure of the molecule, as we experimentally observe. The side view in Fig. 3 shows the N atom forming a bond with the closest Pt (almost "on top"), which forces the C-ring to locate at a slightly shifted bridge site. This N—Pt bond is the strongest, and dominates the adsorption of 4AP on this surface.

This optimal configuration found in the present study for the 4AP molecule on the Pt(111) surface, with the central aromatic ring lying flat on a surface Pt—Pt "bridge", is in excellent agreement with that reported by Liu *et al.* for benzene (Bz) molecules on Pt(111) [42], yielding an adsorption distance between the lowest C atoms and the substrate of 2.08 Å and an adsorption energy of around -1.8 eV, as well as with the experimental adsorption distance evidenced by Wander *et al.* for Bz/Pt(111) of 2.02 ± 0.02 Å [43]. A summary of the results obtained is presented in Table 1.

Additionally, in order to investigate the effect of temperature in the structural rearrangement of the previous RT configuration, we have undertaken molecular dynamics (MD) calculations by including an environmental thermal bath of 300 K. For that purpose, each non-fixed atom α is given a random initial velocity v_α according to a Maxwell–Boltzmann distribution for a given temperature T (300K in this case), such that $\langle V_\alpha^2 \rangle = 3K_BT/2m_\alpha$, where m_α is the mass of each atom involved in the structure. The result of the MD simulations reveals that, at RT, after 100 fs (100 MD steps) a thermally induced HO—C stretching phonon is activated in the 4AP molecule leading to the loss of the whole -OH functional group. This information has been used to obtain the ground-state structure of the molecule on the Pt(111) surface once the OH moiety is removed. Once again, the three previously mentioned non-equivalent on-surface configurations were relaxed, and the same configuration as in the previous case was obtained, with the central ring lying on a Pt—Pt "bridge". The resulting optimal structure is shown in the bottom-left- panel of Figure 3. In

this case the distance between the lowest C atoms of the molecule and the substrate, still lying quite flat on the surface, increases to 2.56 Å, whilst the adsorption energy is substantially reduced to a value of 1.06 eV (see Table 1).

This finding provides some interesting evidence that the two types of molecule observed when depositing 4AP molecules on Pt(111) may be attributed to: i) on-surface 4AP molecules once they have lost the hydrogen atoms of the hydroxyl moieties; and ii) molecules that have lost the whole –OH group by the effect of temperature. Additional molecular dynamics (MD) calculations by including environmental thermal baths with T > 300 K shows the loss of the whole –OH groups, and subsequent loss of hydrogen atoms of the amine groups upon increasing temperature.

In order to justify the aforementioned hypotheses, we have carried out a series of theoretical STM-imaging simulations for both types of molecules on Pt(111). Figure 3 shows the theoretically obtained STM images for both types of molecules on Pt(111) under the same conditions as the experiments (constant-current: I_{tunnel}=0.2 nA and V_s=+0.8 V). In the top-right panel it can be observed that an excellent correlation exists between the first set of molecules appearing in the STM images showing a one-blob morphology, and the theoretical STM image simulated for the 4AP molecules with no hydrogen atoms in the hydroxyl groups on the Pt(111) surface. A one-blob oval structure is located on the whole molecule and, besides the morphological agreement, the measured long and short axis distances of the blob obtained both theoretically and experimentally are identical. On the other hand, the 4AP molecules that show a two-blob structure seem to correspond to AP deposited molecules that have lost the OH moiety due to the effect of temperature. Here the comparison between experimental and theoretical STM images is remarkable (see bottom-right panel of Figure 3). In this case the theoretical STM image (with the molecule geometry superimposed) reveals that the small blob is associated with the $C-NH_2$ bond, whilst the large blob seems to correspond with the dangling bond remaining in each molecule after losing the –OH group, which accommodates charge migrated from internal charge redistribution. This agrees with the fact that the C atom losing the –OH group has increased its distance from the Pt substrate, which is evidence of an excess of charge. Experiment shows that the coexistence ratio between both sets of molecules is around 50%, which at RT seems to be independent of the dose of the deposited molecules.

From the theoretically diluted 4AP(-H)/Pt(111) configuration, discussed above, where the interaction between neighboring molecules could be considered as negligible, we have obtained interesting insights about the molecule-surface interaction. Now the preferential adsorption site and energetics for the 4AP(-H)/Pt(111) in the (2√3×2√3)R30° phase experimentally observed for saturation coverages (see Figure 4) is addressed. For this purpose the unit cell was modelled by a repeated slab geometry (as explained in Section 2) with a size of (9.7×9.7) Å^2, each containing one 4AP(-H) molecule. Once again, we have fully relaxed the aforementioned three non-equivalent starting configurations. The result of the calculations reveals that for this ordered phase the 4AP(-H) molecules once again prefer to locate at the "bridge" adsorption site, lying flat on the surface at a perpendicular distance of around 2.09 Å between the lowest C atoms and the Pt substrate, compared with 2.07 Å for the dilute phase. We have found that the geometry does not manifest any substantial

variation with respect to that found in the dilute phase. From the theoretical optimization, the long axis of the molecule still remains parallel to a direction forming a 30° angle with the main crystallographic directions of Pt(111), without any azimuthal reorientation after the optimization process. The adsorption energy for this configuration is slightly higher (-1.99 eV per molecule) than for the dilute phase case (-1.78 eV), which justifies the tendency of the molecules to rearrange within this more compact (although still sparse) $(2\sqrt{3}\times2\sqrt{3})R30°$ configuration. This may be explained in terms of two issues: i) an emerging weak and repulsive electrostatic interaction between neighboring molecules, and ii) surface depolarization effects arising from a more dense molecular packing, that could induce the molecules to form a slightly stronger anchor with the surface. This means that a theoretically predicted charge transfer from the molecule to the surface of about 0.2 e⁻. This value is slightly lower, 0.18 e⁻, for the molecule that has lost the –OH. Once again DFT+D calculations show that the origin of this interaction is quite chemical, and covalent bonds arise between C and N atoms of the 4AP molecules and the Pt atoms of the substrate in the same way as for the dilute phase. The STM calculated apparent height for the molecules in the diluted and ordered phases is 1.1 and 1.2 Å, respectively, values in excellent agreement with that of 0.9 Å obtained from experimental STM images.

We would like to remark that the strong molecule-surface interaction anchors the molecule to the surface and drives the on-surface orientation in the same way for all the studied cases, impeding any possible rotational or spinning movement, as was reported for interfaces exhibiting interactions of electrostatic nature [44].

Additionally, we have undertaken theoretical STM-imaging simulations for this more compact $(2\sqrt{3}\times2\sqrt{3})R30°$ 4AP(−H)/Pt(111) configuration. The right panel of Figure 4 shows the theoretically obtained STM image calculated under the same conditions as in the experiments (constant-current: I_{tunnel}=0.2 nA and V_s=+0.8 V). Again, a one-blob oval structure is located on each molecule with no visible intramolecular resolution (see Figure 3). Nevertheless, for this more compact phase, the one-blob structure seems to lose its oval shape, with a slight decrease in the length of the long axis of the molecule on the side of the −O groups, resulting in a more rounded morphology than in the previous dilute case. This finding may justify somehow the aforementioned emerging repulsive electrostatic interaction between neighboring molecules and the depolarization effects arising from the denser molecular packing.

In order to induce on-surface chemically driven structural rearrangements of the deposited 4AP layer, the temperature of the system was sequentially increased. Beyond 420 K significant changes occurred to the organic layer (see Figure 5). At this annealing temperature the ordered $(2\sqrt{3}\times2\sqrt{3})R30°$ domains, detected at RT by LEED and STM experiments, vanish. The structural adlayer reorganization indicates that the molecules can undergo on-surface diffusion during thermal treatment. STM images show molecules with two different heights. The molecules now have an apparent height of (2.6 ± 0.5) Å, a value approximately three times higher than that measured at RT (0.9 ± 0.1) Å. After the annealing, in some regions of the sample, coexistence of bright and dim molecules can be observed. Importantly, STM not only captures this significant change in the height of most of the molecules, but also the bright molecules appear to lose the internal structure seen at

RT (see Figure 1), which is now replaced by a more rounded structure. The combination of these factors provides evidence for a significant change in the molecular structure induced by the thermal treatment. In most cases the molecular structures can be clearly delimited, and each bright protrusion can be attributed to a single molecule. This observation seems to be related to the fact that most 4AP molecules have lost one of the functional groups, most likely to be the −OH as discussed below.

Nevertheless, the most striking difference between the organic surface morphology at RT and after annealing is the formation of what appear to be short, linear, single molecular structures, as observed in Figure 5 (left side). Importantly, these new short chain structures were not detected by STM at RT, so it is clear that they are a molecular product obtained by the thermal treatment. These are characterized by short linear segments followed by bifurcations. A standard methodology for detecting a new coupling between molecules on surfaces is to measure the distance between the molecules with STM [5, 45,46]. The average distance between every blob is about (6.5 ± 1) Å, value significantly lower than that obtained at RT by LEED, (9.6 Å) and STM (9.4 ± 0.5) Å. This short value compared with the ordered phase of Figures 1 and 5 suggests that the 4AP have undergone a chemical reaction in which $4 - 5$ molecules have linked together.

While Ihm et al. reported a temperature of around 500 K for the loss of O atoms in related molecules [38] our XPS data (Fig. 2) shows that after annealing the O1s core level peak disappears, and that ascribed to N 1s is now spread over a wider energy range. Both results affirm that the −OH group has been completely eliminated and that the amino group has suffered transformation into a range of different N-environments induced by the loss of one or two H-atoms from the amine groups [47–49]. This last evidence concurs with the information provided by the aforementioned theoretical MD simulations at T=400 and 500 K, which manifest subsequent dehydrogenations of the molecular amine groups once the molecules have lost the hydroxyl groups.

Compiling all the aforementioned information (XPS, STM) we can propose a tentative atomic model for the oligomers shown in figure 5 (central panel). On the STM image we have superimposed a DFT optimized model of a short chain polyaniline structure, which closely matches the STM image. At the right hand side of the image we show the calculated STM image. Our simulated STM image, obtained under the same conditions as in the experiment, manifests visible protrusions associated to each carbon ring and dim zones separating such protrusions, which are associated to the NH groups linking the rings. The comparison between the experimental evidence and the simulated image is very good, not only in the morphology, but also in the inter-protrusion distance (5.8Å). Albeit the XPS spectra of the N1s core level peak indicate an intricate mixture of different chemical species, we have selected −NH- instead of −N= because of energetic considerations. Moreover, the fact that the oligomer structure is not linear is consistent with the angular distortion of the R-NH-R bond, which in our optimized model is about 135°. On the other hand, the observed STM apparent height increase upon oligomer formation could indicate an electronic decoupling of these species with respect to the individually adsorbed molecules.

4 Conclusions

In summary, merging the information obtained thus far, some useful information about the thermally-induced coupling process of 4AP on Pt(111) can be extracted. As starting point, it was shown that at RT already about half of the molecules deposited on the Pt substrate have lost the H atom of the hydroxyl moiety, and the rest of the molecules have completely lost the hydroxyl group. Additionally, it was indicated by XPS that as the temperature increases above 420K, all 4AP molecules have lost the −OH group. This is in agreement with the reduction in the distance between molecules along the linear structures that appear after the thermal treatment (Figure 5). Thus, it is suggested that thermally "activated" molecules can diffuse on the surface and link to other molecules through either partial or full dehydrogenation of the amine groups. Thus, the STM images of Fig. 5 could indicate, for the first time, the formation of short oligomeric chains from 4AP building blocks. It is clear that further research on the coupling reactions of 4AP molecules on similar surfaces is required, in particular for elucidating the configuration of the final products and its implications as a novel route to the controlled formation of macromolecular chains on a surface.

Supplementary Material

Refer to Web version on PubMed Central for supplementary material.

Acknowledgements

References

1. Méndez J, López MF, Martín-Gago JA. Chem Soc Rev. 2011; 40:4578–4590. [PubMed: 21670802]

2. Sanchez-Sanchez C, Orozco N, Holgado JP, Beaumont SK, Kyriakou G, Watson DJ, Gonzalez-Elipe AR, Feria L, Fernández Sanz J, Lambert RM. J Am Chem Soc. 2015; 137:940–947. [PubMed: 25531937]

3. Pinardi AL, Otero-Irurueta G, Palacio I, Martinez JI, Sanchez-Sanchez C, Tello M, Rogero C, Cossaro A, Preobrajenski A, Gómez-Lor B, Jancarik A, et al. ACS Nano. 2013; 7:3676–3684. [PubMed: 23506342]

4. Björk J, Hanke F. Chem A Eur J. 2014; 20:928–934.

5. Gao H, Held PA, Knor M, Mück-Lichtenfeld C, Neugebauer J, Studer A, Fuchs H. J Am Chem Soc. 2014; 136:9658–63. [PubMed: 24937642]

6. Shchyrba A, Martens SC, Wäckerlin C, Matena M, Ivas T, Wadepohl H, Stöhr M, Jung Ta, Gade LH. Chem Commun. 2014; 50:7628–7631.

7. Cirera B, Zhang Y-Q, Björk J, Klyatskaya S, Chen Z, Ruben M, Barth JV, Klappenberger F. Nano Lett. 2014; 14:1891–1897. [PubMed: 24564910]

8. Sun Q, Zhang C, Li Z, Kong H, Tan Q, Hu A, Xu W. J Am Chem Soc. 2013; 135:8448–8451. [PubMed: 23706147]

9. Russell JC, Blunt MO, Garfitt JM, Scurr DJ, Alexander M, Champness NR, Beton PH. J Am Chem Soc. 2011; 133:4220–4223. [PubMed: 21370872]

10. Franc G, Gourdon A. Phys Chem Chem Phys. 2011; 13:14283–14292. [PubMed: 21552604]

11. Bieri M, Nguyen M-T, Gröning O, Cai J, Treier M, Aït-Mansour K, Ruffieux P, Pignedoli Ca, Passerone D, Kastler M, Müllen K, et al. J Am Chem Soc. 2010; 132:16669–16676. [PubMed: 21043454]

12. Treier M, Richardson NV, Fasel R. J Am Chem Soc. 2008; 130:14054–14055. [PubMed: 18826313]

13. Gourdon A. Angew Chem. 2008; 47:6950–6953. [PubMed: 18683834]

14. Beaumont SK, Kyriakou G, Lambert RM. J Am Chem Soc. 2010; 132:12246–12248. [PubMed: 20715838]

15. Kanuru VK, Kyriakou G, Beaumont SK, Papageorgiou AC, Watson DJ, Lambert RM. J Am Chem Soc. 2010; 132:8081–8086. [PubMed: 20491472]

16. Kyriakou G, Beaumont SK, Lambert RM. Langmuir. 2011; 27:9687–9695. [PubMed: 21449570]

17. Beaumont SK, Kyriakou G, Watson DJ, Vaughan OPH, Papageorgiou AC, Lambert RM. J Phys Chem C. 2010; 114:15075–15077.

18. Salavagione HJ, Arias J, Garcés P, Morallón E, Barbero C, Vázquez JL. J Electroanal Chem. 2004; 565:375–383.

19. Salavagione HJ, Arias-Pardilla J, Pérez JM, Vázquez JL, Morallón E, Miras MC, Barbero C. J Electroanal Chem. 2005; 576:139–145.

20. Pinardi AL, Martínez JI, Jan a ík A, Stará IG, Starý I, López MF, Méndez J, Martín-Gago JÁ. Chem Commun. 2014; 50:1555–1557.

21. Horcas I, Fernández R, Gómez-Rodríguez JM, Colchero J, Gómez-Herrero J, Baro aM. Rev Sci Instrum. 2007; 78:013705. [PubMed: 17503926]

22. Lewis JP, Jelínek P, Ortega J, Demkov Aa, Trabada DG, Haycock B, Wang H, Adams G, Tomfohr JK, Abad E, Wang H, et al. Phys Status Solidi B. 2011; 248:1989–2007.

23. Giannozzi P, Baroni S, Bonini N, Calandra M, Car R, Cavazzoni C, Ceresoli D, Chiarotti GL, Cococcioni M, Dabo I, Dal Corso A, et al. J Phys Condens Matter. 2009; 21:395502. [PubMed: 21832390]

24. Grimme S. J Comput Chem. 2006; 27:1787–1799. [PubMed: 16955487]

25. Barone V, Casarin M, Forrer D, Pavone M, Sambi M, Vittadini A. J Comput Chem. 2009; 30:934–939. [PubMed: 18785153]

26. Perdew JP, Chevary JA, Vosko SH, Jackson KA, Pederson MR, Singh DJ, Fiolhais C. Phys Rev B. 1992; 46:6671–6687.

27. Vanderbilt D. Phys Rev B. 1990; 41:7892–7895.

28. Monkhorst HJ, Pack JD. Phys Rev B. 1976; 13:5188–5192.

29. Methfessel M, Paxton AT. Phys Rev B. 1989; 40:3616–3621.

30. Blanco JM, González C, Jelínek P, Ortega J, Flores F, Pérez R. Phys Rev B. 2004; 70:085405.

31. Blanco JM, Flores F, Pérez R. Prog Surf Sci. 2006; 81:403–443.

32. Zhuang SX. Chinese Chemical Lett. 1996; 7:661.

33. Myers AK, Benziger JB. Langmuir. 1989; 5:1270.

34. Richardson NV, Hofmann P. Vacuum. 1983; 33:793–796.

35. Davies PR, Edwards D, Richards D. J Phys Chem B. 2004; 108:18630–18639.

36. Masini F, Ning Y, Li Z, Lægsgaard E, Besenbacher F, Linderoth TR. Chem Commun. 2013; 49:8665–8667.

37. Otero G, Biddau G, Ozaki T, Gómez-Lor B, Méndez J, Pérez R, Martín-Gago JA. Chem A Eur J. 2010; 16:13920–13924.

38. Ihm H, White JM. J Phys Chem B. 2000; 104:6202–6211.

39. Bebensee F, Svane K, Bombis C, Masini F, Klyatskaya S, Besenbacher F, Ruben M, Hammer B, Linderoth T. Chem Commun. 2013; 49:9308–93010.

40. Bebensee F, Svane K, Bombis C, Masini F, Klyatskaya S, Besenbacher F, Ruben M, Hammer B, Linderoth TR. Angew Chemie Int Ed. 2014; 53:12955–12959.

41. Schmitz CH, Schmid M, Stefan G, Steinr H, Gottfried JM, Sokolowski M. J Phys Chem C. 2011:18186–18194.

42. Liu W, Carrasco J, Santra B, Michaelides A, Scheffler M, Tkatchenko A. Phys Rev B. 2012; 86:245405.

43. Wander A, Held G, Hwang RQ, Blackman GS, Xu ML, de Andres P, Van Hove MA, Somorjai GA. Surf Sci. 1991; 249:21–34.

44. Sanchez-Sanchez C, Lanzilotto V, Gonzalez C, Verdini A, de Andres PL, Floreano L, Lopez MF, Martin-Gago JA. Chem - A Eur J. 2012; 18:7382–7387.

45. Fan Q, Wang C, Han Y, Zhu J, Hieringer W, Kuttner J, Hilt G, Gottfried JM. Angew Chem. 2013; 52:4668–4672. [PubMed: 23512581]

46. Eichhorn J, Strunskus T, Rastgoo-Lahrood A, Samanta D, Schmittel M, Lackinger M. Chem Commun. 2014; 50:7680–7682.

47. Tan KL, Tan TG, Kang ET, Neoh KG. Phys Rev B. 1989; 39:8070–8073.

48. Chen Y, Kang E, Neoh K. Appl Surf Sci. 2002; 185:267–276.

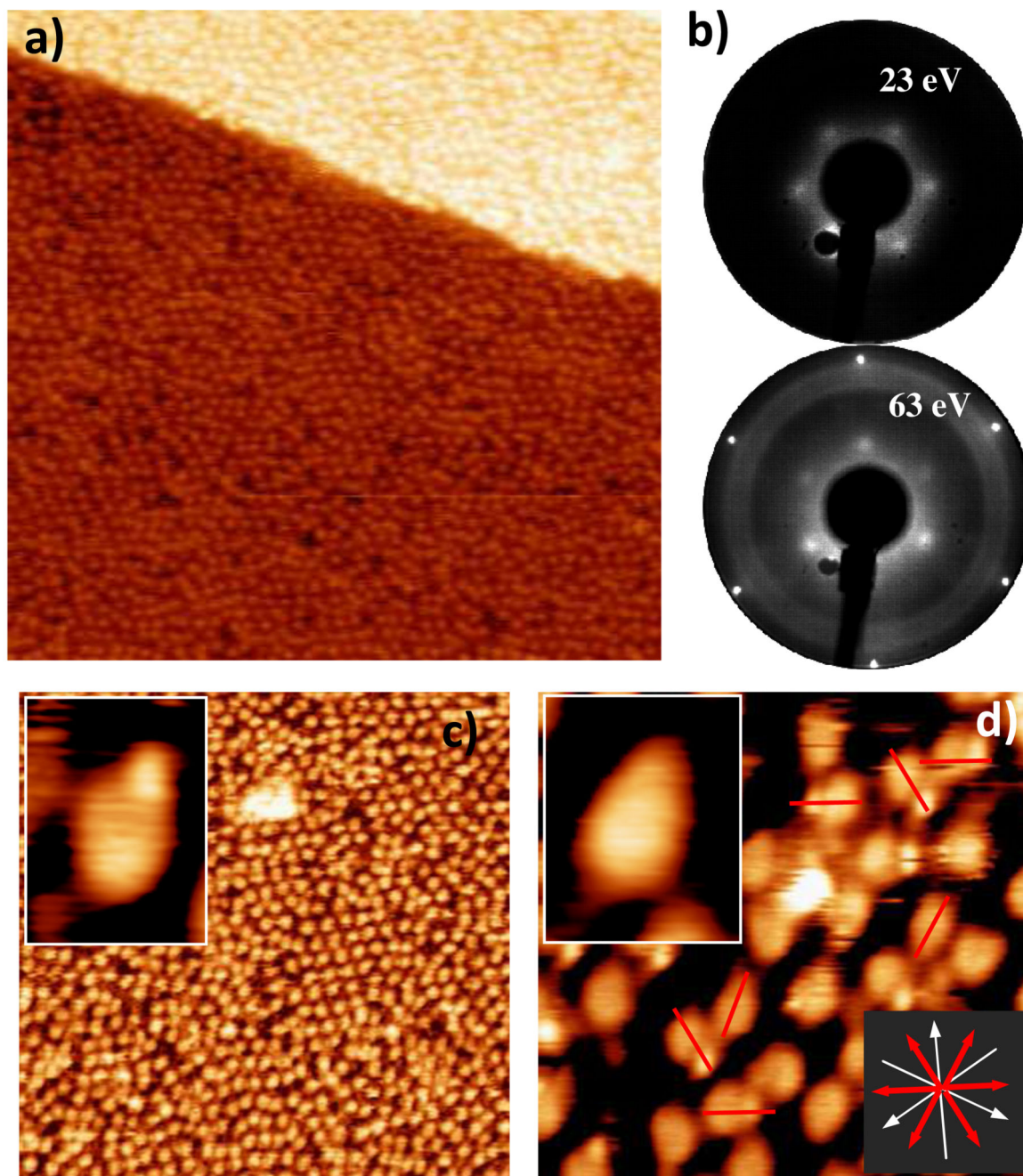49. Hennig C, Hallmeier KH, Szargan R. Shynthetic Met. 1998; 92:161–166.

Figure 1.
STM images of 4AP on Pt(111) at RT and saturation coverage. (a) STM image of the overall surface topography (35×35)nm^2. (b) LEED patterns at different energies corresponding to the emergence of a $\left(2\sqrt{3}\times2\sqrt{3}\right)$R30° superstructure. (*c*) STM image (25×25)nm^2. where small regions with local order are appreciated. (*d*) STM image (6×6) nm^2. The long axis of the molecules (red arrows) are rotated 30° with respect to the main crystallographic directions of the Pt(111) surface (white arrows). Two different internal molecular structures

are observed at RT (top-left insets in panels c and d). STM images were acquired under constant-current scanning conditions for I_{tunnel}=0.2 nA and V_s=+0.8 V.
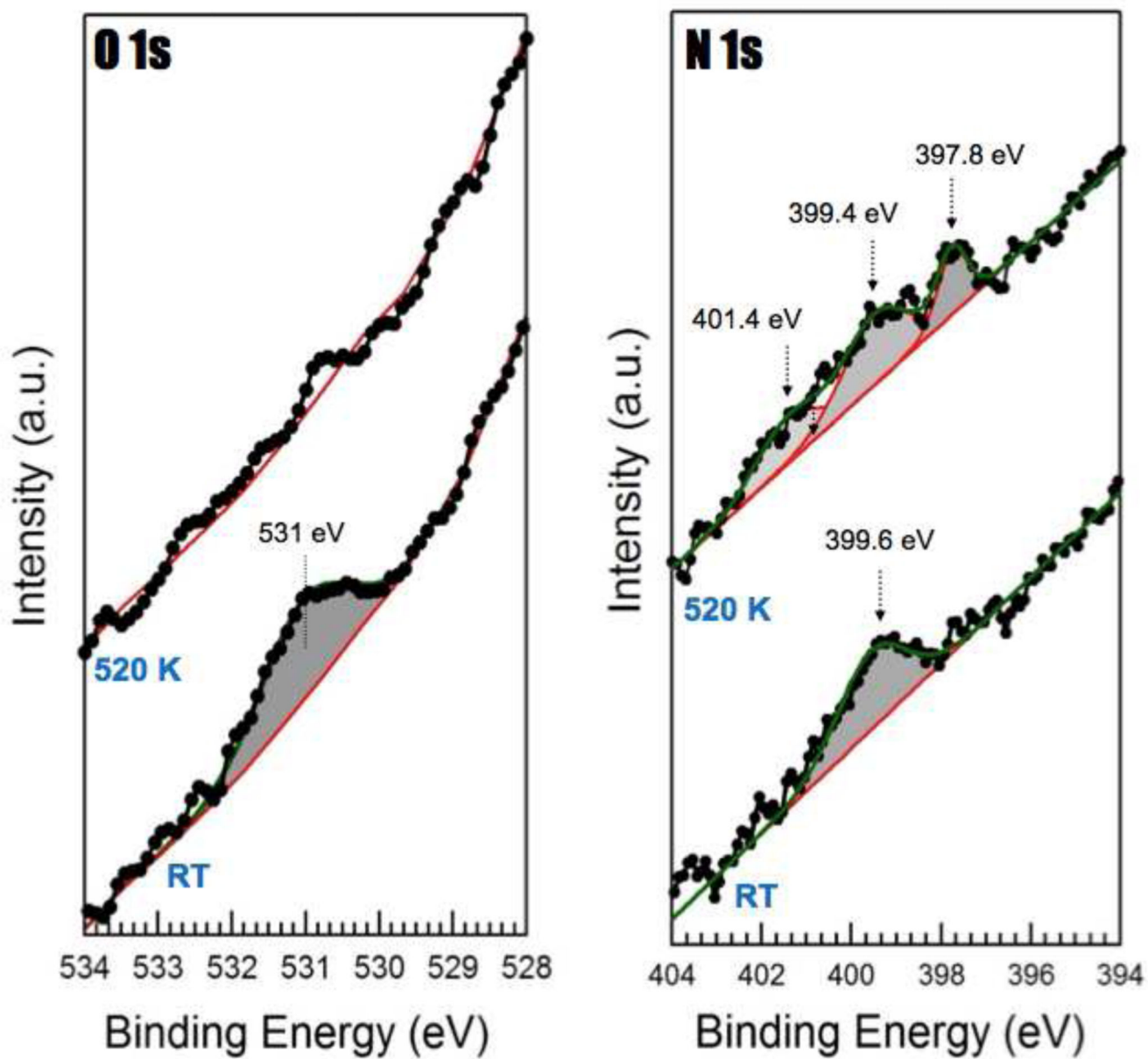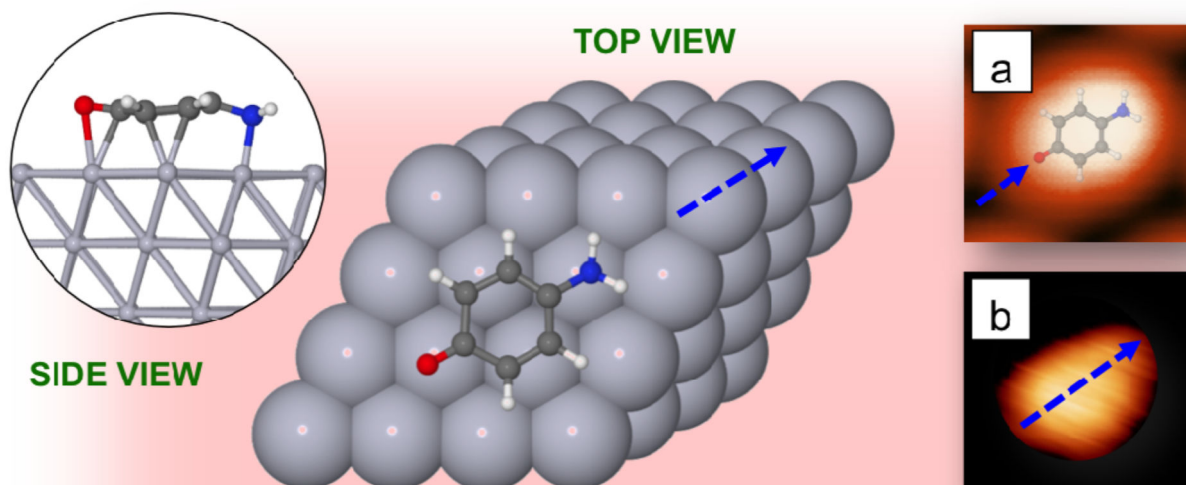
Figure 2.
O 1s and N 1s core level peaks obtained for 1 ML of 4AP on Pt(111) at RT (lower spectra) and after heating the samples to 520 K (upper spectra).

Aminophenol / Pt(111) (-H lost) – *Dilute phase (4×4)*

TOP VIEW

SIDE VIEW

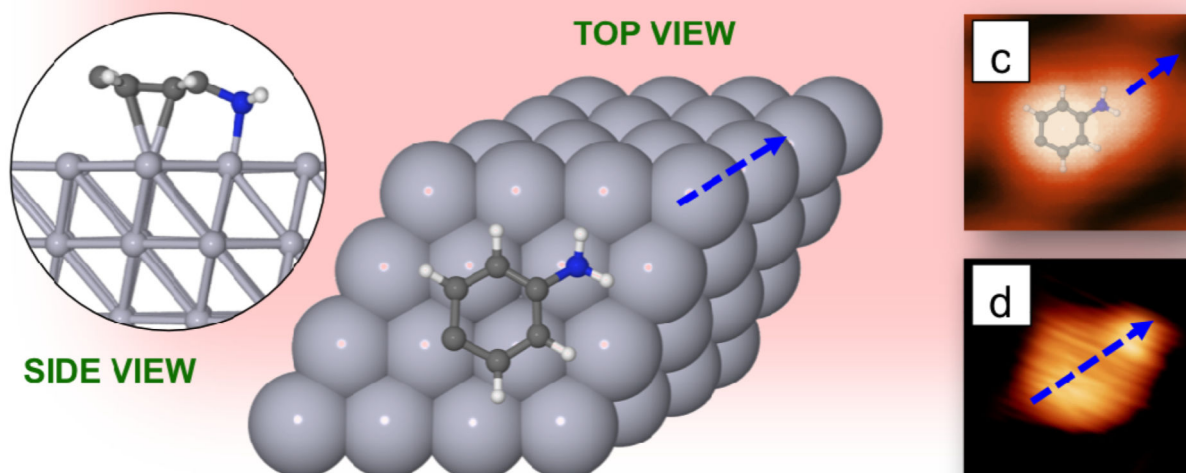# Aminophenol / Pt(111) (-OH lost) – *Dilute phase (4×4)*

TOP VIEW

SIDE VIEW

Figure 3.

Top and side views of the optimal surface geometry for a dilute (4×4) phase for: (top panel) 4AP molecule on Pt(111) after loss of the hydrogen atom of the hydroxyl group ; (bottom panel) 4AP molecule on Pt(111) after loss of the whole −OH group. (a) Computed and (b) experimental STM image for the 4AP molecule on Pt(111) after loss of the hydrogen atom of the hydroxyl group . (c) Computed and (d) experimental STM image for the AP molecule on Pt(111) after loss of the −OH group. The STM images were obtained under constant-current conditions (I_{tunnel}=0.2 nA and V_s=+0.8 V). The blue-dashed arrow indicates a direction rotated 30° w.r.t. the main Pt(111) crystallographic directions. The atomic coordinates can be found as on-line Supplementary Material
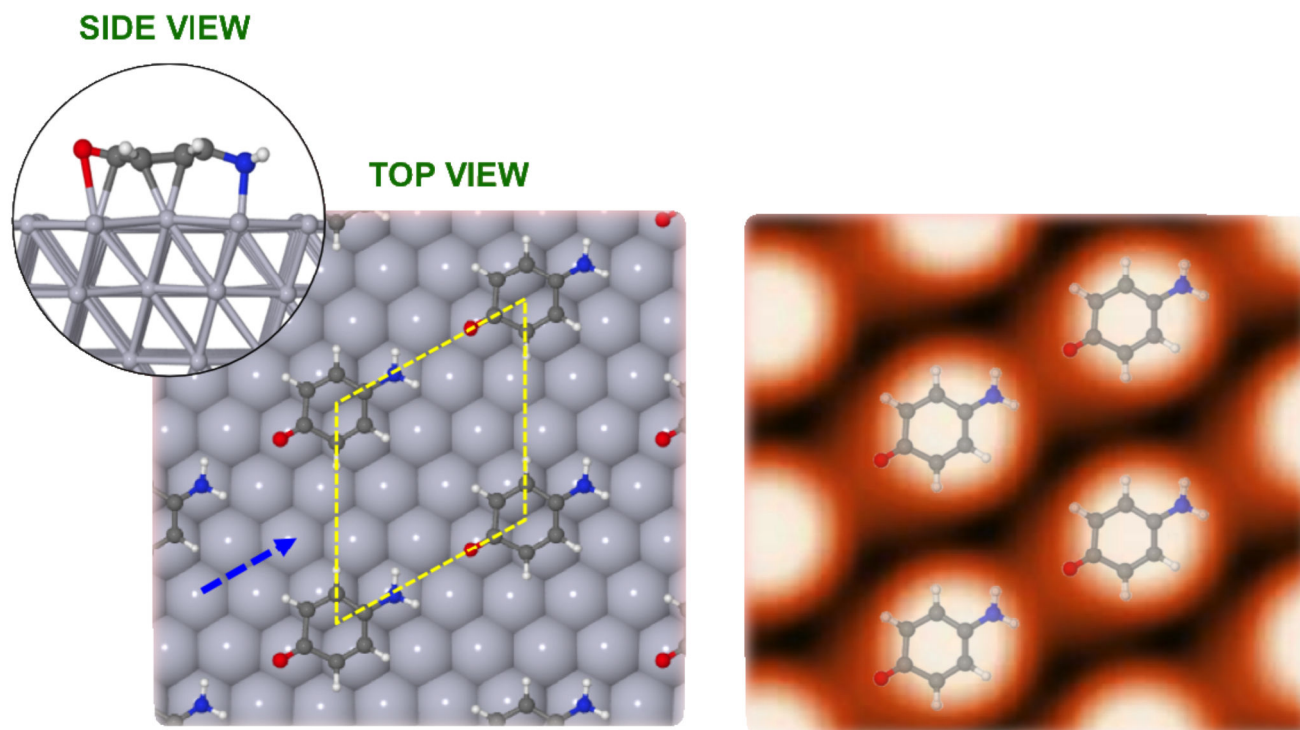
Figure 4.
(Left) Top and side views of the optimal surface geometry for the compact ($2\sqrt{3}\times2\sqrt{3}$)R30° 4AP(-H)/Pt(111) configuration. (Right) Computed STM image for the 4AP(-H)/Pt(111) configuration shown in left-panel. STM image has been computed under constant-current conditions (I_{tunnel}=0.2 nA and V_s=+0.8 V). Blue-dashed arrow indicates a direction rotated 30° w.r.t. the main Pt(111) crystallographic directions.
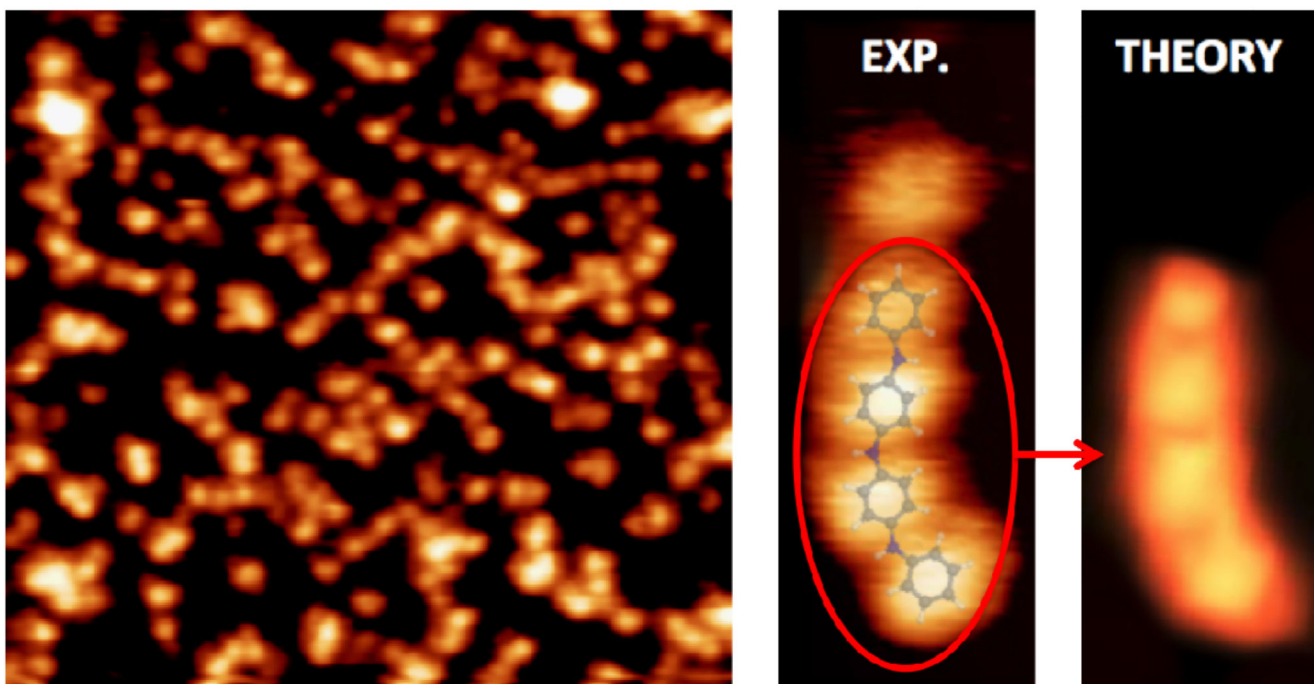
Figure 5.
left side: STM image obtained recorded after annealing at 420 K the Pt(111) surface dosed at saturation coverage of 4AP molecules. The apparent height of these molecular features is (2.6 ± 0.5) Å. Centre image: zoom on a oligomeric chain.(14.6×14.6) nm^2; (1.6×3.3) nm^2. A DFT optimized model has been superimposed on the STM image. Right side image: STM calculation of the experimentally observed oligomer.

Table I

Distance between the lowest C atoms of the molecule and the Pt substrate, d_{C-M} (in Å), adsorption energy per molecule, E_{ads} (in eV), and the same values for benzene on Pt(111) taken from refs. [42,43], for the 4AP(-H)/Pt(111) and 4AP(-OH)/Pt(111) in a dilute (4×4) phase (see Figure 2), and for the 4AP(-H)/Pt(111) in the close-packed (2 3×2 3)R30° phase (see Figure 3),

	This work		Reported for benzene	
	d_{C-M} (Å)	E_{ads} (eV)	d_{C-M} (Å)	E_{ads} (eV)
(4×4) 4AP(-H)onPt (RT)	2.07	−1.78	2.08 [42] / 2.02 [43]	−1.8 [42]
(4×4) 4AP(-OH)onPt (RT)	2.56	−1.06		
(2 3×2 3)R30° 4AP(-H)onPt (RT)	2.09	−1.99		